

Cross-layer Framework for Energy Harvesting-LPWAN Resource Management based on Fuzzy Cognitive Maps and Adaptive Glowworm Swarm Optimization for Smart Forest

Hancong Wang, *Student Member, IEEE*, Yin Wu, Qiang Ni, *Senior Member, IEEE* and Wenbo Liu

Abstract—Modern forestry research and management increasingly rely on precise environmental data. Presently, Low Power Wide Area Networks (LPWANs) offer potential advantages for such field monitoring tasks. However, their applicability requires enhancements in aspects such as power consumption, transmission range, data rate, and consistent quality of service. This paper introduces a novel control model emphasizing cross-layer collaboration, aiming to bolster the efficiency and reliability of Energy Harvesting (EH) LPWANs within the context of intelligent forest management. By employing the influential factors of EH-LPWAN as conceptual nodes, an innovative fuzzy cognitive map (FCM) can be designed. The interrelations among these concepts become instrumental in developing the cross-layer optimization model, addressing various objectives and tackling overlapping constraints. To further refine the model's efficacy, an adaptive glowworm swarm optimization (AGSO) driven dynamic FCM method is presented to ascertain the conceptual weights while facilitating real-time updates. Preliminary results manifest a noteworthy enhancement in communication range by 40.2%, a betterment in packet delivery accuracy by 19%, and an extension in the LoRaWAN's projected lifespan by 33.8% during scenarios with diminished EH rates. It's evident that the energy self-sustainability of EH nodes coupled with the data handling capacity of the entire network fully aligns with the stringent real-time and consistency criteria mandated for meticulous forest observation.

Index Terms—LPWAN, energy harvesting, cross layer control, fuzzy cognitive map, glowworm swarm optimization, smart forest

I. INTRODUCTION

Forest, integral to Earth's terrestrial ecosystems, are increasingly interfacing with advancements in technology, specifically the Internet of Things (IoT). Within this technological advancement, Low-power wide-area networks (LPWANs) have emerged as a notable IoT innovation, distinguished by characteristics such as minimal energy requirements, cost-effectiveness, and extensive range coverage [1] [2]. However, the integration of LPWANs in diverse operational contexts, coupled with the escalating deployment of IoT devices, presents pronounced challenges, particularly regarding data transmission capacities. The crux of these challenges lies in the burgeoning number of IoT devices introduced into var-

ious environments. This expansion, while instrumental for enhanced data collection and monitoring, also instigates significant strain on the finite wireless resources integral to LPWAN functionality [3]. The ensuing contention between the rapidly proliferating devices and the constrained resources manifests as a principal constraint impeding LPWAN performance. Addressing this dilemma necessitates the development of resource allocation strategies that are both robust and efficient. These strategies must focus on the judicious management of several resources, encompassing wireless channels, allocation of time slots, device energy conservation, and the optimization of hardware computing abilities. Consequently, fostering reliable data transmission for a multitude of devices hinges on these sophisticated resource management method-

This work is an extended version of an IEEE WCNC'2023 paper (url: <https://ieeexplore.ieee.org/document/10119004>), and was supported in part by the National Natural Science Foundation of China (NSFC) under Grant No.32171788, No.31700478; Jiangsu Provincial Government Scholarship for Overseas Studies under Grant JS-2018-043; Qing Lan Project of Jiangsu Colleges; Innovation and Entrepreneurship Training Program for College Students in Jiangsu Province under Grant 202310298043Z. (Corresponding author: Yin Wu).

Hancong Wang, Yin Wu are with the College of Information Science and Technology, Nanjing Forestry University, Nanjing, 210037, China (e-mail: hancong@njfu.edu.cn; wuyin@njfu.edu.cn).

Qiang Ni is with the Infolab21, School of Computing and Communications, Lancaster University, Lancaster, LA1 4WA, United Kingdom (e-mail: q.ni@lancaster.ac.uk).

Wenbo Liu is with the College of Automation Engineering, Nanjing University of Aeronautics and Astronautics, Nanjing, 211106, China (wenboliu@nuaa.edu.cn).

ologies, establishing this as a pivotal research domain within LPWAN studies.

Conversely, the heterogeneity of environmental conditions and application specifications necessitates the deployment of LPWANs in contexts with distinct attributes. Urban regions, for instance, are fraught with dense impediments like buildings, significantly impeding wireless signal propagation [4]. This scenario mandates the incorporation of numerous relay apparatuses to bolster communication dependability [5]. In contrast, rural or open-field conditions pose a different set of challenges: the exorbitant costs associated with manual battery substitutions for terminal apparatuses underscore the criticality of prolonging network operational life. Herein, energy harvesting (EH) techniques have crystallized as indispensable, primarily due to their capacity to curtail operational interruptions and optimize energy utilization [6]. The varying demands and operational hurdles in these settings underscore the necessity for adaptable, scenario-specific solutions. These conditions compel a strategic re-evaluation of resource allocation, hardware deployment, and energy management methodologies, tailored to accommodate the unique constraints and requirements of each environment. By embracing this adaptability, it becomes feasible to enhance LPWAN's operational efficiency and reliability across an array of application scenarios.

EH-LPWAN plays a pivotal role in extending network operational duration and epitomizes the essence of eco-friendly communication. Nonetheless, the EH process at the sensor nodes is fraught with inconsistencies and unpredictability, largely attributable to environmental factors and the constraints of existing hardware [7]. The imperative to judiciously utilize the harvested energy for effective data transmission poses a critical conundrum in the EH-LPWAN sphere [8]. Present studies on resource stewardship and data transfer in EH-LPWAN typically focus on isolated layers of the network protocol stack [9]-[11]. However, this approach overlooks the integral fact that efficient data transfer depends on the collaborative functionality of all protocol stack layers [12]. Hence, there's an emerging consensus on the potential benefits of cross-layer optimization in EH-LPWAN, a strategy poised to substantially ameliorate network efficacy.

This research introduces an innovative cross-layer framework designed to optimize network efficiency within EH-LPWAN. Utilizing a sophisticated mathematical approach, specifically the Fuzzy Cognitive Map (FCM), it is possible to create a parameterized depiction of the underlying causal processes inherent in wireless communications [13]. Complementing this, the study employs an adaptive glowworm swarm optimization (AGSO) technique, responsible for the precise calculation of relevant weights. The culmination of this methodology is poised to significantly contribute to the establishment of a forestry IoT management system, characterized by its heightened reliability and sensitivity.

Our contributions are described briefly below:

- 1) Tailoring to the distinct features of forestry LPWAN, the research has fabricated a cross-layer optimization and control model, underpinned by the careful election of particular determinants that exert influence within the

system.

- 2) The introduction of a novel FCM technique plays a pivotal role in establishing connections among various cross-layer parameters. This methodology goes beyond conventional FCM approaches by introducing a distinctive coefficient node seamlessly integrated with standard input, output, and concept nodes, thus accommodating diverse network correlation requirements.
- 3) Enhancement of the existing AGSO algorithm is executed, specifically tailored for the newly proposed FCM model. Empirical evidence highlights its superior efficacy, particularly in terms of convergence, precision, and stability, when compared with alternative swarm intelligence algorithms.
- 4) By strategically focusing on achieving a balanced equilibrium between EH rate and LPWAN network performance metrics, the FCM mechanism demonstrates proficiency in dynamically moderating key control variables such as node energy expenditure. This contributes to optimizing data throughput efficiency.

The rest of this paper is organized as follows: Commencing with Section II, a succinct review and deliberation concerning extant studies in the domain of cross-layer optimization within EH-LPWAN are undertaken, followed by an exposition of the envisaged system-level framework architecture. Progressing to Section III, an exhaustive elucidation of the operational steps characterizing the EH-FCM mechanism is tendered. Advancing into Section IV, readers encounter methodical descriptions of both the simulation processes and the ensuing comparative experiments. Culminating in Section V, the document encapsulates all preceding discussions with insightful concluding observations.

II. RELATED WORKS

In recent years, a surge of interest from scholarly and industrial circles has been directed towards cutting-edge LPWAN technologies. These include, but are not limited to, LoRaWAN [14], Sigfox [15], Weightless [16], and D7AP [17], all of which operate within the ISM band, utilizing an unlicensed spectrum that obviates the need for formal authorization. Their comparative advantage, specifically their minimal energy consumption relative to their licensed cellular counterparts, has catalyzed their adoption in forestry IoT endeavors. For instance, research spearheaded by Victor Matasov et al. involved a pioneering exploration, monitoring eco-physiological parameters across 16 distinct trees to quantify ecosystem service indicators pertinent to climate, air quality, and water regulation [18]. Another study by Gilles Callebaut et al. assessed the reach of LoRa links and formulated path loss models based on empirical data gathered in forested locales [19]. Further innovation was demonstrated by Mike O. Ojo et al., who engineered and appraised a LoRa packet generator tailored to both moderately dense and highly dense forestry conditions [20]. Moreover, a novel wildfire detection mechanism leveraging Sigfox technology is documented in [21]. In a separate study, researchers advocated for NB-Fi as the

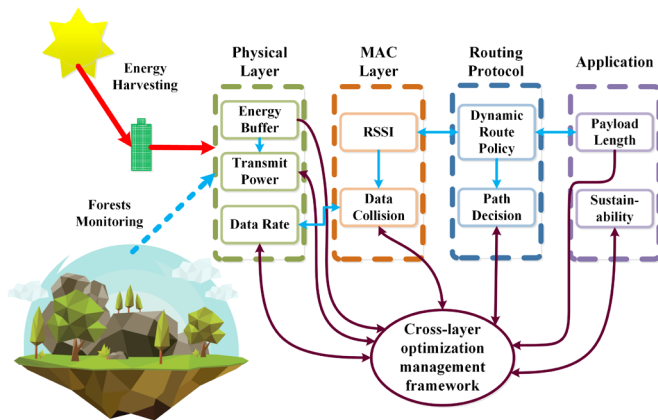


Fig. 1. Cross-layer cooperation model of EH-LPWAN.

optimal solution catering to expansive agricultural estates [22]. Nonetheless, a conspicuous gap remains in the extant literature: there is scant consideration given to the seasonal dynamics within forest ecosystems, let alone the growth trajectories of individual trees. This oversight represents a critical disconnect for long-term field operations featured in contemporary studies. Consequently, there is an imperative to conceive, refine, and implement a judicious LPWAN resource stewardship framework—one marked by heightened efficiency and formidable resilience—for the enduring surveillance of ecological systems.

Energy harvesting techniques coupled with joint layer optimization strategies stand at the forefront of enhancing the operational efficacy of wireless sensor networks, a principle increasingly applied within the LPWAN spectrum. Specific advancements include the work by Binbin Su et al., focusing on maximizing energy efficiency in LoRa networks through the integrated approach of user scheduling, assigning spreading factors (SF), and calibrating transmit power [23]. A. Abouzarkhanifard et al. designed a MEMS energy harvesting module based on transfer learning algorithm [24] [25] and Parsi B et al. optimized the energy harvesting strategy of micropump in combination with genetic algorithm [26]. These studies provide good approaches to the design of EH modules for sensors. In another development, Benjamin Karg et al. employed predictive control strategies tailored to navigate the inherent limitations of the Sigfox network [27]. J. Finnegan et al. explored the feasibility of utilizing ambient RF energy to power LoRaWAN sensor nodes boundary [28]. Further contributions to this field are evident, such as a comprehensive cross-layer framework that encompasses energy models, downlink communications, and adaptive data rates, as assessed in [25]. A distinct approach by Carmen Delgado et al. involved the formulation of a Markov model designed explicitly to depict the operational dynamics of LoRaWAN devices devoid of battery dependencies [26]. Dalibor Purkovic et al. contributed by engineering a communication protocol optimized for energy efficiency, specifically for EH-LPWAN sensor modules [27]. Moreover, an innovative environmental monitoring solution featuring an autonomous Sigfox sensor node was introduced in [28]. Despite these strides, there remains a pronounced need for intensified research geared towards optimizing EH-LPWAN,

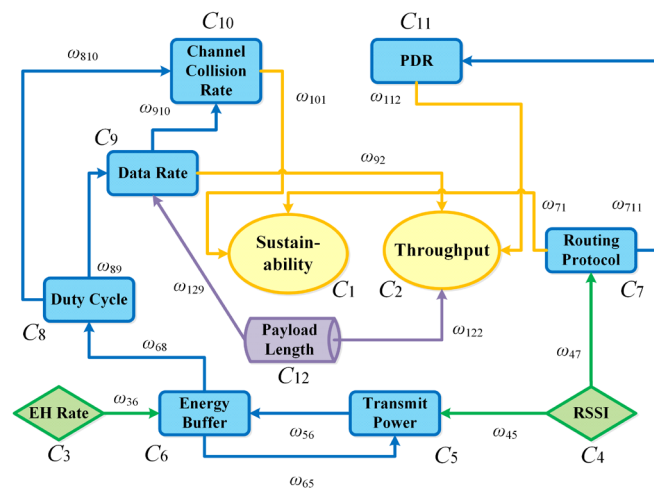


Fig. 2. FCM Model of EH-LPWAN for a smart forest monitoring.

particularly under the influences of fluctuating transmission channels. This need stems from the inherent tension between divergent constraints and multiple operational objectives, such as balancing energy-neutral operations with transmission power, harmonizing data throughput with channel utilization, and juxtaposing propagation loss against routing protocols. Therefore, meticulous cross-layer studies are imperative, aimed at bolstering the sustainability of EH nodes defined as maintaining residual energy above operational thresholds [29] and enhancing network throughput, warranting precise investigation and rigorous evaluation.

III. THE PROPOSED FCM OPTIMIZATION METHOD

This segment delves into the intricate process of cross-layer optimization within EH-LPWAN, utilizing the Fuzzy Cognitive Map (FCM) approach. It encapsulates a comprehensive structure of the FCM methodology, highlights the application of the AGSO algorithm in determining the relative weights across concept nodes, and discusses the execution of control strategies under diverse operational scenarios.

A. Framework for Cross-layer Optimization

Addressing the nuanced communication requisites of forestry, particularly within the constraints of semi-fixed observation site topologies as outlined in monitoring criteria [30], there exists significant potential to leverage the intricate dynamics of LPWAN. This includes the physical link condition, the MAC layer's channel disposition, and insightful routing information, all achieved through sophisticated inter-layer coordination. By dynamically tuning system variables that exhibit mutual real-time interdependencies, the strategy paves the way for a collaborative optimization paradigm, facilitating end-to-end data conveyance within an EH-LPWAN framework. The model of such cross-layer collaborative control is depicted in Fig.1. Contrastingly, in traditional settings, amplifying the transmission power of a solitary LPWAN node theoretically bolsters communication reliability. Yet, this escalation inadvertently exacerbates the ambient noise at the physical stratum, potentially undermining the data transfer capabilities of adjacent nodes. Furthermore, condensing the transmission

intervals at the MAC layer ostensibly augments real-time responsiveness, albeit at the risk of escalating data collision occurrences, thereby curtailing reliability. Within routing paradigms, the primary objective revolves around striking a balance between maximizing network throughput and curbing energy consumption. In scenarios where traditional single-hop topologies grapple with sustaining an energy-balanced mode, there emerges a pressing need to explore multi-hop routing anchored on criteria like the Received Signal Strength Indicator (RSSI) complemented by the evolving energy harvest trajectory. Concurrently, at the application layer, it becomes evident that payload size significantly governs the quantum of transmitted data. This interplay mandates an exploration of its ramifications on sustainability metrics and sensitivity thresholds. Hence, the proposed cross-layer modulation approach calls for an integrated assessment, consolidating parameters such as the rate of energy harvest, power designated for transmission, channel availability, the integrity of the link, routing determinations, and data initiation points. This integration is aimed at forging a collaborative approach to optimize service quality, leading to a self-regulating, smart forestry communication framework.

B. Structure of the Proposed Framework

FCM stands as a streamlined, intuitive graphical illustration, serving as an effective inferential tool for intricate systems, characterized by an assemblage of concepts (variables within a system) alongside their interrelations (causality amongst variables) [31]. An archetypal FCM encompasses four integral components, expressed as $G = (C, E, X, f)$. Herein $C = (C_1, C_2, \dots, C_N)$ amalgamates the entirety of concept nodes within an FCM, encompassing input nodes, output nodes, inferential nodes, and the novel coefficient node introduced in this study. N signifies the cumulative count of nodes. Moreover, $E: (C_i, C_j) \rightarrow \omega_{i,j}$ is a dedicated mapping function where $C_i, C_j \in C$, $\omega_{i,j} \in [0,1]$, signifying the degree of causality exerted by node C_i upon node C_j . The function $X: C_i \rightarrow X_i^t$ explicates the value attributed to system node C_i at iteration t ; f is the threshold function to turn X_i^t into numerical value A_i^t , which refers to the active degree of node C_i . This framework, therefore, not only illustrates the intricate interplay between diverse system variables but also quantifies the influence degree, thereby providing a robust mechanism for inference and prediction in complex multi-nodal environments.

Within the scope of this study, the construction of an intricate FCM model is undertaken, integrating various nodes categorized as inputs, outputs, coefficients, and concepts, serving distinct functions within the network's paradigm. In the outlined model, both the EH rate and RSSI status serve as prominent input nodes. On the other hand, the model earmarks system sustainability and data throughput as vital output nodes. Distinguishing this model, the length of the payload is factored in as a coefficient node. In a parallel context, myriad elements like transmission power, the rate of channel collisions, the chosen routing protocol, and an ensemble of six other components are integrated as conceptual nodes. This integration enhances the robustness of the FCM model illustrated in Fig. 2. Central to the functionality of the EH-FCM

is the equilibrium it strives to uphold between the facets of power utilization and the overarching network efficacy. To this end, FCM initiates adjustments to the values corresponding to C_5 and C_7 , reflecting the metrics of the destination output nodes, namely, throughput and system sustainability. Subsequent to these initial modifications, the model undertakes a recalibration of the remaining nodes' values. This process hinges on established reasoning formulas, culminating in the deployment of these redefined parameters within the tangible operational environment, thereby ensuring an adaptive response to real-time network demands and conditions. It is worth mentioning that the coefficient node does not receive input from other nodes and differs from the input node in that its value is fixed in the current task. The value of ordinary input node (such as RSSI) changes over time, while the value of coefficient node remains constant in the field application scenario. Therefore, different EH-FCM should be trained according to the preset payload length, and the parameter value set in this paper will be presented in Section V.

This research delineates a structured approach by identifying a specific set of concept nodes, collectively represented as $\{C\} = \{C_1 \text{ Sustainability, } C_2 \text{ Throughput, } C_3 \text{ EH rate, } C_4 \text{ RSSI, } C_5 \text{ Transmit Power, } C_6 \text{ Energy Buffer, } C_7 \text{ Routing Protocol, } C_8 \text{ Duty Cycle, } C_9 \text{ Data Rate, } C_{10} \text{ Channel Collision Rate, } C_{11} \text{ Packet Delivery Ratio, PDR, } C_{12} \text{ Payload Length}\}$. Critical to the framework's architecture is the employment of a weight set $\{\omega_{i,j}\}$, $i \in [1,11], j \in [1,11]$ symbolizing the causative correlation between any two entities C_i and C_j within the predefined system. Thus, the study necessitates the formation of an incidence matrix, denoted as W , premised on these interdependencies. This matrix becomes instrumental in encapsulating the intensity and directionality of influences amongst the variables, laying the groundwork for subsequent analytical procedures and insights.

$$W = \begin{bmatrix} \omega_{1,1} & \omega_{1,2} & \dots & \omega_{1,12} \\ \omega_{2,1} & \omega_{2,2} & \dots & \omega_{2,12} \\ \vdots & \vdots & \ddots & \vdots \\ \omega_{12,1} & \omega_{12,2} & \dots & \omega_{12,12} \end{bmatrix} \quad (1)$$

Upon establishing the values within matrix W and discerning the system's current status through the $\{C\}$ set at an iteration t , it becomes feasible to project the subsequent communication state of LPWAN at the instant $t+1$. This predictive step is crucial, enabling proactive adjustments in network strategies.

$$A_i(t+1) = f(A_i(t) + \sum_{i=1, j \neq i}^N A_i(t) \cdot \omega_{i,j}) \quad (2)$$

The function $f(\cdot)$ stands as the designated threshold mechanism, defined as follows:

$$f(x) = 1 - \frac{1}{1 + e^{-\tau x}} \quad (3)$$

where τ serves as a modulating parameter within the threshold function, thereby altering its configuration. Empirical data may guide the appropriate selection of diverse τ values, adjusting the function's shape correspondingly. It becomes imperative to recognize that the various concept nodes operate on different

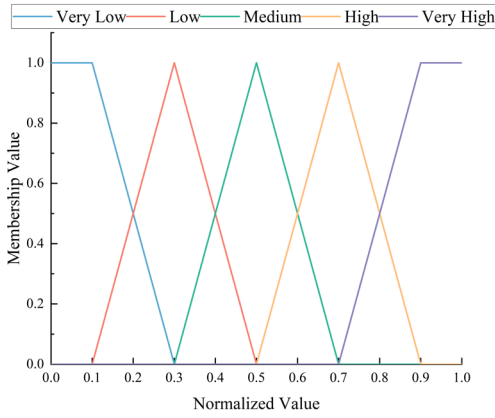


Fig. 3. Membership function for concept nodes.

scales and dimensions, necessitating a preliminary standardization process for their respective values. This normalization ensures consistency and comparability, streamlining the integration within the analytical framework.

$$A_i = 1 - \frac{1}{1 + e^{\frac{2[z_i(t) - z_i^{\max}(t) + z_i^{\min}(t)] - z_i^{\max}(t) - z_i^{\min}(t)}{z_i^{\max}(t) - z_i^{\min}(t)}}}} \quad (4)$$

In the process of normalization, $z_i^{\max}(t)$ and $z_i^{\min}(t)$ represent the maximum and minimum threshold values of the real-world measurement $z_i(t)$ corresponding to the concept node C_i at any given instance t . Concurrently, z^{\max} and z^{\min} denote the extremities of the value spectrum for the concept node exhibiting the broadest range within the system at the identical temporal marker. This establishment of parameters warrants that the subsequent relational equation holds true:

$$z^{\max}(t) - z^{\min}(t) = \max_i [z_i^{\max}(t) - z_i^{\min}(t)] \quad (5)$$

Utilizing the outcomes derived from equation (4), it becomes feasible to standardize the actual values inherent to each concept node, ensuring their confinement within the (0, 1) interval. This standardization facilitates the assignment of a precise hierarchical position relative to the membership function delineated in Fig. 3. Diverging from this, certain qualitative nodes, exemplified by C_1 and C_7 , defy direct quantification. These nodes require an interpretative categorization spanning five distinct echelons - Very Low through Very High. This stratification aligns with the fuzzy control theory, correlating sequentially with numerical approximations of 0.1, 0.3, 0.5, 0.7, and 0.9.

C. Solution of Concept Weights

In addressing the computational methodology for W , the study introduces a refined version of the adaptive glowworm swarm optimization algorithm. The core of the algorithm is to set the weight between each node in FCM as the coordinates of a glowworm individual in a high-dimensional space. Assuming that there are several glowworms in the high-dimensional space, their positions can be iterated by calculating the luciferin concentration and other related information between different individuals. The final position where the glowworms converge is the optimal solution of concept weight. This enhanced technique involves a glowworm, designated as i , possessing

the capability to navigate within an N-dimensional expanse. The locational vector of this particular glowworm, pertinent to a specific iteration phase, is expressible as follows:

$$X_i(t) = (X_{i1}, X_{i2}, \dots, X_{iN}) \quad i, t \in \mathbb{N} \quad (6)$$

In the intricate dynamics of the adaptive glowworm swarm optimization, each glowworm assumes a pivotal role by exuding a specific quantum of luciferin, serving as a beacon to its proximate counterparts. The luciferin concentration attributable to glowworm i , specific to the iteration phase denoted as t , is subject to computation in the ensuing manner:

$$l_i(t) = \max \{0, (1 - \rho)l_i(t-1) + \gamma F[X_i(t)]\} \quad (7)$$

Within the framework of the adaptive glowworm swarm optimization algorithm, two primary factors influence the luciferin dynamics critical to the movement and interaction of the glowworms. Firstly, the parameter ρ stands as the luciferin attenuation coefficient, instrumental in dictating the depletion rhythm of residual luciferin within each glowworm. Concurrently, γ represents the luciferin enhancement ratio, pivotal in adjusting the luciferin concentration, contingent on $F[X_i(t)]$, the specific value derived from the target function.

Focusing on the exploration behavior, glowworms initiate a search protocol, prioritizing peers characterized by a superior luciferin concentration relative to their own within a designated sensory field. Should the sensory radius affiliated with glowworm i during iteration t phase be expressed as $r_i^d(t)$, the subsequent assemblage of perceivable neighboring glowworms to which i is privy can be delineated as follows:

$$N_i(t) = \left\{ j : \|X_j(t) - X_i(t)\| < r_i^d(t) \cap l_j(t) < l_i(t) \right\} \quad (8)$$

Assuming that there are multiple elements in the set $N_i(t)$, glowworm i will randomly select an individual j from the set according to the probability ratio of luciferin value and move to it. Suppose that the probability of i moving to j is $P_{ij}(t)$, and the position of i is updated to $X_i(t+1)$ after the move, then:

$$P_{ij}(t) = \frac{l_j(t)}{\sum_{k \in N_i(t)} l_k(t)} \quad (9)$$

$$X_i(t+1) = X_i(t) + s \left[\frac{X_j(t) - X_i(t)}{\|X_j(t) - X_i(t)\|} \right] \quad (10)$$

In this context, the determination of the adaptive step size, denoted as s , emerges as a critical factor, attainable through the ensuing computational approach:

$$s(t) = s_{\max} \cdot e^{-p \left(\frac{t}{t_{\max}} \right)^\lambda} + s_{\min} \quad (11)$$

where λ acts as a scaling factor crucial for determining the adaptive step size, operating within an established spectrum defined by s_{\max} and s_{\min} , indicating the maximal and minimal step extents, respectively. Concurrently, p serves as the modification determinant adjusting the step size precision.

The search path of Levy flight can improve the ability of algorithm in the global search space, expand the search range and make it easier for the glowworm to jump out of the local extrema. This paper introduced Levy stable distribution, a non-Gaussian stochastic process to increase the reliability of the algorithm, equation (10) can be improved as:

$$X_i(t+1) = X_i(t) + s \left[\frac{X_j(t) - X_i(t)}{\|X_j(t) - X_i(t)\|} \right] + \delta \cdot \text{sign}(\text{rand} - 0.5) \oplus \text{Levy} \quad (12)$$

where a and b follow a normal distribution

$$\text{Levy} \sim \frac{\mu}{|v|^{1/\zeta}} \quad (13)$$

$$\begin{cases} \mu \sim N(0, \sigma_\mu^2) \\ v \sim N(0, \sigma_v^2) \end{cases} \quad (14)$$

$$\begin{cases} \sigma_\mu = \left\{ \frac{\Gamma(1+\beta) \sin(\pi \cdot \beta / 2)}{\Gamma[(1+\beta) / 2] 2^{(\beta-1)/2} \beta} \right. \\ \left. \sigma_v = 1 \right. \end{cases} \quad (15)$$

Within the specified boundaries of β , which extend from 0 to 2, the conventional choice tends to be 1.5. δ is the step factor, and rand is a random factor obeying uniform distribution on [0,1]. The expression $\text{sign}(\text{rand} - 0.5)$ in equation (7) assumes the role of randomizing direction. Meanwhile, 'Levy', derived from equation (6), signifies the stochastic step, epitomizing the movement of fireflies—an erratic promenade influenced by the heavy-tailed probability distribution. This movement pattern accentuates the algorithm's prowess in securing optimal resolutions. Nonetheless, the integration of Levy flights enhances the algorithm's capacity for a comprehensive global search. This amplification, however, mildly compromises its proficiency in local exploration during the algorithm's advanced iterations. Specifically, the convergence precision may experience a decrement when the necessity for an intensive search within a confined region arises, and the algorithm persists in a state favoring extensive global probing.

To address the issue of suboptimal local solutions resulting from the Levy flight strategy's implementation, this study introduces a crossover operator incorporating elite elements. Within the realm of swarm intelligence optimization algorithms, elite members of the population play a crucial guiding function, harboring the potential to uncover the optimal solution. The iterative process's efficacy is often enhanced as the population gravitates toward these elite entities, simplifying the trajectory toward the optimal solution. Nonetheless, an overemphasis on convergence might stagnate the algorithm, trapping it within local optima. In the context of genetic algorithms, an elite strategy is employed, earmarking high-performing individuals for crossover, while simultaneously preserving these superior members. This method not only augments the diversity among potential solutions but also fosters conditions conducive to transcending local optima. It maintains superior individuals, guiding the population evolution toward an optimal state. Given that elite solutions often surpass their non-elite counterparts at specific gene expression loci, their involvement in crossover operations propagates advantageous gene segments, a technique that starkly contrasts with traditional crossover applications that exclusively preserve elite members throughout iterations. This propagation amplifies the gene pool's quality, particularly those genes integral to elite individuals, thereby

heightening the likelihood of a population poised for substantial solution enhancement. In light of these insights, this study advocates for a crossover operator enriched with elite participation. This innovative operator engages non-elite members in crossover activities with the most proficient elite candidates available, safeguarding superior offspring and predecessors to supplant the original non-elite fireflies. Despite its simplicity, this operator proves potent, accelerating the update velocity of individual firefly positions and facilitating the acquisition of comparatively superior solutions with greater ease. The initial phase of this process involves the meticulous selection of elite members embedded within the population.

$$X_{\text{best}}(t) = X_i(t), F[X_i(t)] \leq F[X_j(t)], \forall j \in \{1, 2, \dots, N\} \quad (16)$$

Second, the renewed non-elite individuals are selected and their genes are randomly crossed with those of the elite individuals to produce new individuals.

$$\begin{cases} X_{\text{best}}(t) = (X_1, X_2, \dots, X_n) \\ X_{\text{renew}}(t) = (Y_1, Y_2, \dots, Y_n) \end{cases} \quad (17)$$

$$\begin{cases} X_{r1}(t) = (X_1, X_2, \dots, X_k, Y_{k+1}, Y_{k+2}, \dots, Y_n) \\ X_{r2}(t) = (Y_1, Y_2, \dots, Y_k, X_{k+1}, X_{k+2}, \dots, X_n) \end{cases} \quad (18)$$

Finally, the resulting offspring were evaluated and the better individuals were selected to replace the original ones.

$$X_{\text{renew}}(t) = \begin{cases} X_{r1}(t), F[X_{r1}(t)] \leq \min\{F[X_{r2}(t)], F[X_{\text{renew}}(t)]\} \\ X_{r2}(t), F[X_{r2}(t)] \leq \min\{F[X_{r1}(t)], F[X_{\text{renew}}(t)]\} \\ X_{\text{renew}}(t), \text{else} \end{cases} \quad (19)$$

According to the above derivation, glowworms with higher luciferin generally have a strong attraction effect only on glowworms with smaller relative distance. However, this mutual attraction often exists to guide other individuals around to move to positions with poor solution quality, which leads to the problem that the algorithm shows low accuracy and tends to fall into the local optimal solution and converge too early. Therefore, this paper adds a screening mechanism to ensure that the glowworms entering the next iteration are all improved and qualified individuals. The position update formula is improved as follow:

$$X_i(t+1) = \begin{cases} X_i(t), F[X_i(t)] > F[X_i(t+1)] \\ X_i(t) + s \left[\frac{X_j(t) - X_i(t)}{\|X_j(t) - X_i(t)\|} \right], \text{else} \end{cases} \quad (20)$$

The sensory radius's magnitude exhibits a dependence on the count of entities residing within its sensory domain. In scenarios where the glowworm density within the sensory sphere is scant, an augmentation in its sensory radius ensues to facilitate the identification of an increased number of adjacent entities. Conversely, the sensory radius undergoes a contraction. Once positional adjustments transpire, alterations in its sensory radius materialize in a corresponding manner, governed by the subsequent update equation:

$$r_i^d(t+1) = \min\{r_i^s, \max\{0, r_i^d(t) + \xi(n_i - |N_i(t)|)\}\} \quad (21)$$

where ξ symbolizes the rate at which the neighborhood alters, n_i represents the threshold count for the neighborhood-

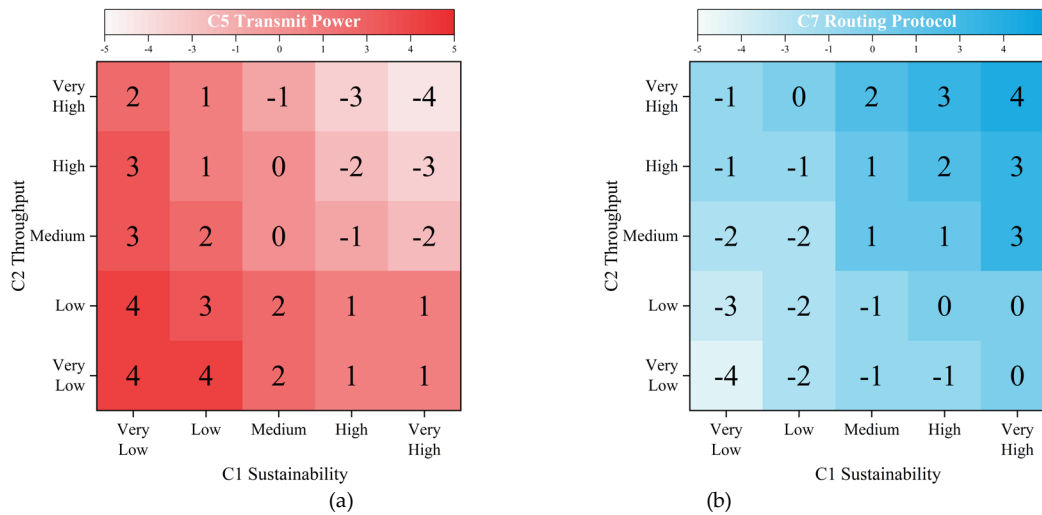


Fig. 4. Fuzzy inference rules based on (a) transmit power and (b) routing protocol.

TABLE I
VARIABLE DEFINITION AND VALUE

Variable Name	Definition	Value
τ	Slope of the threshold function	2
ρ	Luciferin attenuation factor	0.15
γ	Luciferin update rate	2
λ	Scaling factor	2
ξ	Neighborhood change rate	2
α	Loss factor	0.9

confined glowworms, r_i^s is indicative of the glowworms' dynamic decision range, and the constraint $0 < r_i^d(t) < r_i^s(t)$ is upheld. The algorithm's execution concludes either when it achieves the upper limit of iteration cycles or when the function under scrutiny surpasses a predetermined threshold value, upon which the algorithm ceases, rendering the glowworms' coordinates as the sought parameters.

In the study, the application of AGSO centers on ascertaining the inter-nodal concept weights, leading to the representation:

$$X_i(t) = (\omega_{1,1}, \omega_{1,2}, \dots, \omega_{12,12}) \quad (22)$$

$$Error = \frac{1}{P \times T \times N} \sum_{p=1}^P \sum_{t=1}^T \sum_{n=1}^N |A_n^p(t) - \widetilde{A}_n^p(t)| \quad (23)$$

$$F[X_i(t)] = \frac{1}{\alpha \cdot Error + 1} \quad (24)$$

where the term $A_n^p(t)$ signifies the post-FCM reasoning value, contrasting with $\widetilde{A}_n^p(t)$, $\widetilde{A}_n^p(t)$ is the value of the sample used for training.

Acknowledging environmental factors' impact, the fuzzy cognitive graph's predictive outcome may exhibit minor deviations from actual values, necessitating adjustments in the inter-concept nodal weights:

$$\omega_{ij}(t+1) = \omega_{ij} + \varphi(t)[\Delta q_i \Delta q_j - \omega_{ij}(t)] \quad (25)$$

$$\varphi(t) = 0.1 \left[1 - \frac{t}{1.1k} \right] \quad (26)$$

here k corresponds to the numeral indicative of learning phases, adjustable relative to real-world conditions. Δq represents the absolute discrepancy between authentic measurements and FCM inferences. Conclusively, these

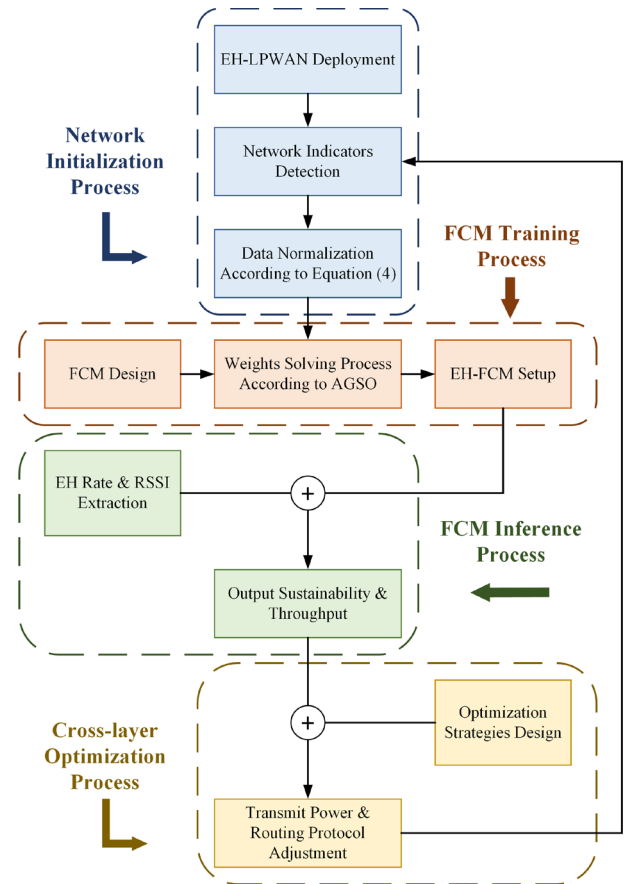


Fig. 5. Operation flow of the proposed cross-layer optimization framework.

recalibrated weights contribute to aligning node values with sustainability and throughput prerequisites, thereby facilitating cross-layer optimization within the network. Pertinent variable values employed in the AGSO algorithm are documented in TABLE I.

D. Cross-layer Optimization Strategy

Considering the EH-FCM framework introduced within this study, optimization of network efficacy necessitates particular

TABLE II
Simulation Parameters

Parameter	Value
Number of Nodes	100 to 500
Gateway	1
Network Size (m ²)	500×500
Spreading Factor	{7, 8, 9, 10, 11, 12}
Bandwidth (kHz)	125
Packet Size (bytes)	42
Data Generation Rate (bps)	1000
Payload Length (bytes)	65
Transmit Power (dBm)	2 to 16
Data Rates (kbps)	0.5 to 37.5
	Rx: 26mAh
Power Consumption	Tx: 26mAh + (Tx power × packet size/data rate)
	Sleep: 0.3μAhr×sleep time
Initial Power	15Ahr

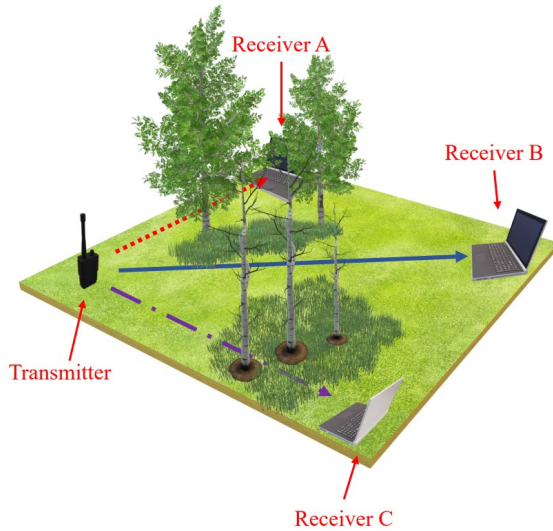


Fig. 6. Attenuation model of forest signal transmission.

attention to the quantifications of concept nodes C_5 and C_7 , with a directive focus on the output nodes C_1 and C_2 . Illustrated in Fig. 4 are the intricate fuzzy inference protocols, where Fig. 4 (a) and (b) detail the mandated operations for C_5 and C_7 , contingent on the respective statuses of C_1 and C_2 . Elucidation extends through the exposition of two distinct scenarios:

Scenario 1: In the context where the statuses of C_1 , C_2 , C_5 and C_7 are delineated as Low, Medium, Very Low, and High correspondingly, strategic modifications become imperative. The approach necessitates elevating C_5 by two strata to achieve a Medium classification while concurrently necessitating the reduction of C_7 intensity by an equivalent magnitude to secure a balanced Medium stature. Such recalibrations are pivotal, enhancing the operative quality of the network infrastructure. This optimization process primarily involves augmenting the potency of the transmission channels and succinctly curtailing the expansiveness of the navigational pathways, thereby fostering a more streamlined and efficient network paradigm.

Scenario 2: In the scenario where the conditions of C_1 , C_2 , C_5 and C_7 are identified as High, Very High, Medium, and Low, respectively, a necessity for immediate recalibration in

the system's parameters emerges. Initially, C_5 is slated for a three-tier reduction; however, constraints limit this adjustment, relegating it directly to the minimal threshold of Very Low. Concurrently, an imperative escalates regarding C_7 , necessitating its elevation by three segments, thus reaching the Very High category. This strategic modulation in system variables leads to a tangible decrement in signal transmission power, a step integral to energy conservation protocols. Furthermore, an extension in the navigation pathway becomes essential, designed to facilitate direct information dispatch towards the gateway. This methodology not only minimizes network congestion but significantly enhances overall network performance quality.

Conclusively, EH-FCM epitomizes a mechanism of fluid adjustments. The stability of the system mirrors the constancy of environmental constituents. Conversely, should these factors undergo substantial alterations, the system possesses the agility to initiate appropriate strategies to mitigate network disruptions. Illustrated in Fig. 5 is the procedural progression of the cross-layer optimization framework introduced within this study.

IV. SIMULATIONS AND EXPERIMENT RESULTS

In this segment, the performance assessment of EH-FCM encompasses four distinct simulations, scrutinizing aspects such as algorithmic convergence, communication caliber, endurance of the network, and the span of communication. The initial phase involved constructing a simulation milieu in MATLAB, grounded on LoRaWANSim, a concept advanced by Marini et al. [32]. Pertinent parameters are delineated in TABLE II. Subsequently, this simulation's deployment for LoRaWAN facilitated the acquisition of essential training time series data, thereby enabling the establishment of EH-FCM through the application of the AGSO algorithm.

This study presents a streamlined interpretation of EH Rate and RSSI. The former segregates into three categories, indicative of the recharging rate's intensity levels: low, medium, and high. A low stratum fails to suffice the sensor's energy requisites, whereas the high echelon not only suffices but also allows surplus energy storage within the battery, with the medium level maintaining a position of equilibrium between these extremes. Contrarily, RSSI signifies the diminution strength of the signal, wherein a low RSSI is synonymous with heightened channel attenuation. The model employed for channel attenuation within this discourse is exhibited hereunder:

$$L_p(d) = L_p(d_0) + 10\zeta \lg\left(\frac{d}{d_0}\right) + X_\sigma \quad (27)$$

In this analysis, the focus pivots to a tailored channel transmission model, conceptualized to ascertain the quantifiable value of ζ , reflective of the intrinsic properties of signal propagation within forested locales. The equation governing this model incorporates several variables: d represents the intervening space between nodes engaged in transmission and reception, d_0 serves as the benchmark distance, $L_p(d_0)$ quantifies path loss experienced at this reference point, ζ stands as the path loss exponent, and X_σ emerges as a variable adhering to the normal distribution

principles. The illustrative aid in Fig. 6 demarcates three distinct scenarios. Under conditions where the receiver, termed ‘A’, is ensconced amidst foliage dense enough to impose shielding, the ζ value escalates, synonymous with high attenuation. Conversely, an unobstructed channel facilitating signal reception at receiver ‘B’ correlates with the nadir in ζ values, indicative of low attenuation. An intermediate scenario prevails for receiver ‘C’, where minimal vegetative obstruction exists, leading to a ζ value that nestles between the high and low extremes, aptly termed moderate attenuation. This model transcends mere theoretical significance by mirroring the cyclical oscillations observed in channel characteristics corresponding to the annual seasons in the subtropical zone of the northern hemisphere. Explicitly, it depicts a moderate attenuation spectrum during the vernal and autumnal equinoxes, a diminished attenuation phase in the hibernal season, and a peak attenuation period in the estival season. These fluctuations owe their periodicity to the seasonal vegetative density variations.

A. Algorithm Performance

This section underscores the efficacy of the introduced AGSO algorithm by juxtaposing it against several established optimization methods, namely, particle swarm optimization (PSO), ant colony optimization (ACO), genetic algorithm (GA), and grey wolf optimization (GWO), in the context of determining the optimal weights for EH-FCM. The experimental protocol mandates a ceiling of 400 iterations. Given the intricacy of the FCM requiring the fine-tuning of 16 distinct weights, the swarm size for each computational approach under consideration aligns with this number, fixed at 16. Adherence to optimal parameter values, as documented in [33]-[36], ensures uniformity in comparative analysis. Iterative progress, depicted in intervals of 20, finds representation in Fig. 7, concentrating on the evolution of the fitness function values.

It can be seen that the AGSO algorithm demonstrates superiority by effectively circumventing the pitfalls of local optimum solutions, a common issue within the conventional GA algorithm framework. This advanced strategy not only mitigates the risk of entrapment in suboptimal performance zones but also garners the pinnacle of fitness values. Conversely, the PSO algorithm exhibits tendencies for premature convergence, attributable to its deficient global exploratory prowess and subpar search methodologies amongst particles. During the advanced phases of evolutionary computation, the GA algorithm’s efficiency markedly deteriorates, resulting in protracted computational times and a propensity for confinement in local optimums. In contrast, the ACO, though successful in eluding local optimality dilemmas, fails to secure commendable fitness values, indicating room for enhancement in its operational mechanics.

B. Communication Quality

Regarding the evaluation of communication efficacy, this study examines four distinct parameters: the rate of channel collisions, network throughput, Packet Delivery Ratio (PDR), and the velocity of data transmission. These metrics are graphically represented from Fig. 8-Fig. 11, respectively. The

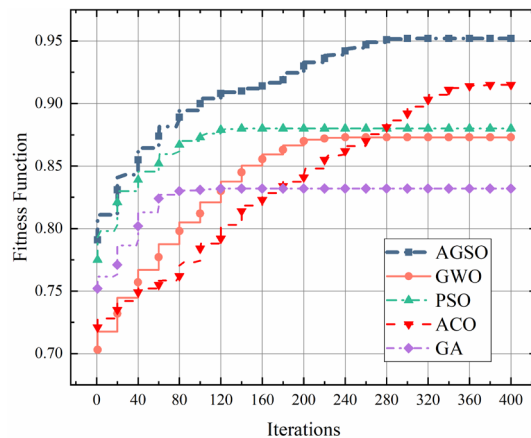


Fig. 7. The fitness values of different optimization algorithms after every 20 iterations.

experimental protocol involves modulating channel attenuation at intervals of 2000 seconds throughout a comprehensive examination span of 12,000 seconds. Concurrently, assessments are made on the network's average performance during these distinct periods. The findings indicate that the LoRaWAN, augmented by EH-FCM, surpasses the conventional LoRaWAN across all tested parameters within identical signal attenuation conditions. Notably, the EH-FCM-enhanced version maintains superior communication quality, even under severe attenuation scenarios, eclipsing the standard model's performance under minimal attenuation conditions. This observation substantiates the potential of EH-FCM in bolstering standard LPWAN to fulfill the stringent wireless communication demands intrinsic to forestry environments.

In the evaluation of channel collision rates, the EH-FCM variant maintains a performance record of under 30% in the majority of scenarios, whereas the standard version exhibits a substantially elevated collision rate, with the peak value approaching 50%. This indicates the enhanced channel resource utilization afforded by EH-FCM. Concerning throughput, the method introduced demonstrates a discernible optimization over the standard version, with an average increase of approximately 4.3%, constituting a notable advancement for LPWAN technologies. Concurrently, in PDR simulations, the EH-FCM framework effectively mitigates the network packet loss rate under pronounced channel attenuation, with a maximum PDR enhancement of roughly 38.2%. In conditions of minimal network channel attenuation, the PDR facilitated by EH-FCM optimization consistently exceeds 75%. Pertinently, forestry IoT necessitates specific communication data rates and real-time responsiveness. Empirical data reveal that the EH-FCM framework substantially elevates the LoRaWAN data rate, thereby enabling nodes, even those situated at extended distances from the gateway, to support high-speed data conveyance.

Subgraphs (a), (b) and (c) in Fig. 8-Fig. 11 individually illustrate performance across diverse EH Rate scenarios. The standard LoRaWAN remains unaffected by this variable, in contrast to the network refined by the EH-FCM framework, which initiates specific measures primarily due to alterations in transmission power. At elevated EH Rates, the EH-FCM

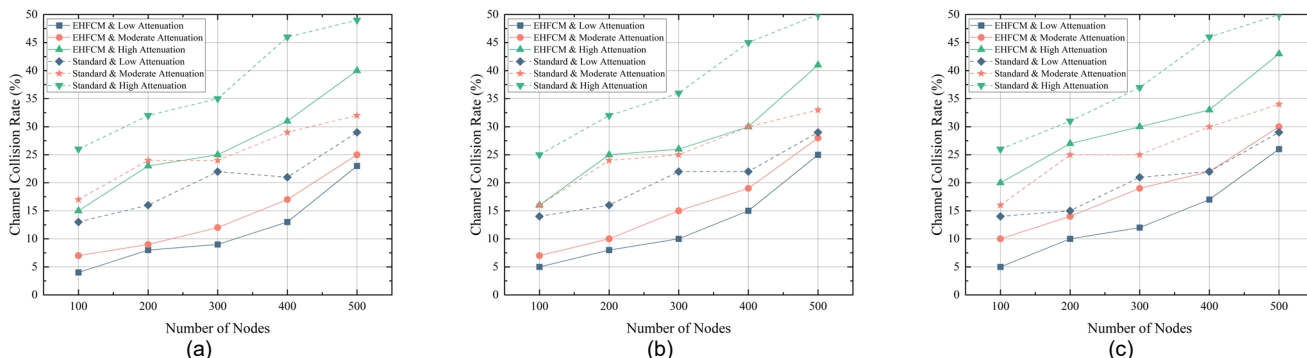


Fig. 8. Channel collision rate of EH-FCM based LoRaWAN and standard LoRaWAN in (a) high EH rate, (b) moderate EH rate and (c) low EH rate scenarios for different number of nodes and channel attenuation degrees.

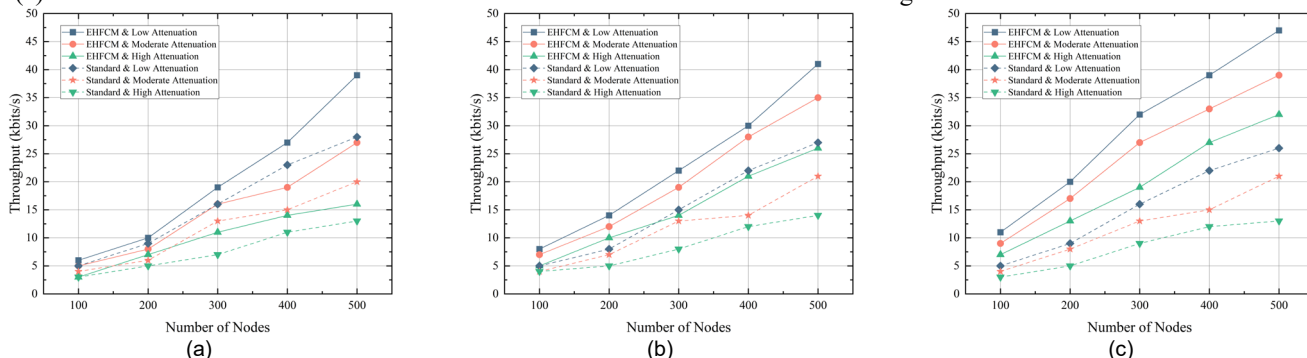


Fig. 9. Throughput of EH-FCM based LoRaWAN and standard LoRaWAN in (a) high EH rate, (b) moderate EH rate and (c) low EH rate scenarios for different number of nodes and channel attenuation degrees.

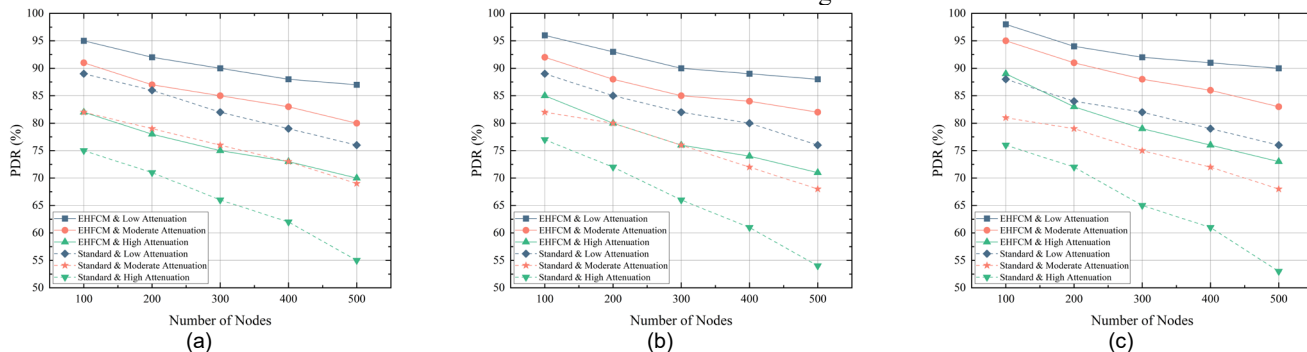


Fig. 10. PDR of EH-FCM based LoRaWAN and standard LoRaWAN in (a) high EH rate, (b) moderate EH rate and (c) low EH rate scenarios for different number of nodes and channel attenuation degrees.

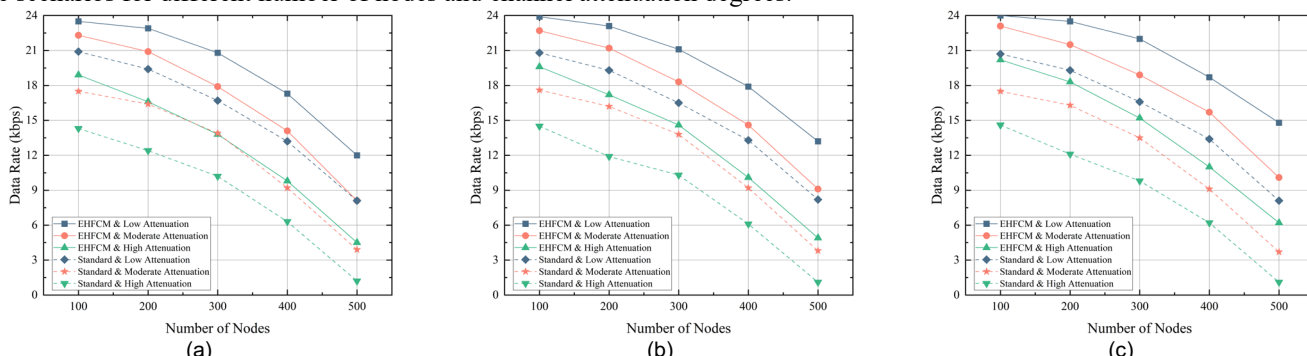


Fig. 11. Data rate of EH-FCM based LoRaWAN and standard LoRaWAN in (a) high EH rate, (b) moderate EH rate and (c) low EH rate scenarios for different number of nodes and channel attenuation degrees.

framework escalates transmission power, eliciting corresponding repercussions on network performance, including increased channel collision rates and data rates. Under these circumstances, EH-FCM implements routing adjustments to mitigate the proliferation of adverse

consequences, subsequently influencing other performance metrics. Collectively, the EH-FCM framework contributes constructively to the enhancement of network performance.

An important observation is that LoRaWAN, when integrated with EH-FCM, exhibits enhanced performance over

its standard counterpart concerning convergence across various levels of channel fading. This enhancement stems from EH-FCM's capability to process input data in a sequential manner based on time series. This continuous method of data handling ensures a more seamless operation compared to its standard counterpart, effectively circumventing instances of abrupt spikes or significant drops in network parameters.

C. Sensor Lifetime

In this analysis, the focus is on simulating the energy utilization across the network, interpreted through the lens of network longevity. The criterion adopted for defining the network's lifespan is the juncture at which 50% of the nodes cease to function. Illustrative Fig. 12 (a), (b) and (c) delineate the longevity of the network under diverse conditions characterized by high, moderate, and low energy harvesting (EH) rates, respectively. Specifically, a scenario with a moderate EH rate is one that experiences a tangible degree of energy influx, albeit insufficient in most instances to counterbalance the energy expenditure incurred during the standard operational activities of the EH-sensors.

The cumulative evidence from the experiments conducted indicates a superior energy management capacity in LoRaWAN systems that integrate EH-FCM, surpassing that of the conventional LoRaWAN framework. This superiority becomes particularly evident under conditions where the network

TABLE III
Statistical Analysis

EHFCM Standard	Low	Moderate	High	Mixed
Max	2793.5	1899.7	1197.7	1585.0
	2384.6	1676.9	1010.4	1332.9
Min	2505.3	1518.9	744.8	1174.3
	1813.3	920.8	200.5	735.9
Mean	2639.9	1711.6	942.3	1405.9
	2059.7	1237.3	613.6	998.7
Variance	7570.7	16637.5	19303.1	15349.7
	29806.9	59817.3	70364.6	41709.1

channel quality deteriorates due to environmental disruptions. In such instances, EH-FCM exhibits a strategic competence in modulating transmission power, contributing significantly to energy conservation. Furthermore, in circumstances involving extensive network scales, EH-FCM demonstrates its efficacy by refining the routing methodology, aiming for the mitigation of channel collisions. This refinement circumvents the rigid tactic of merely escalating the power used for signal transmission, an approach typically associated with standard systems. By doing so, not only is energy efficiency observed, but there is also an enhancement in overall network performance quality. Consequently, in the simulated environments structured for this analysis, it is evident that the LPWAN optimized with EH-FCM manifests a performance

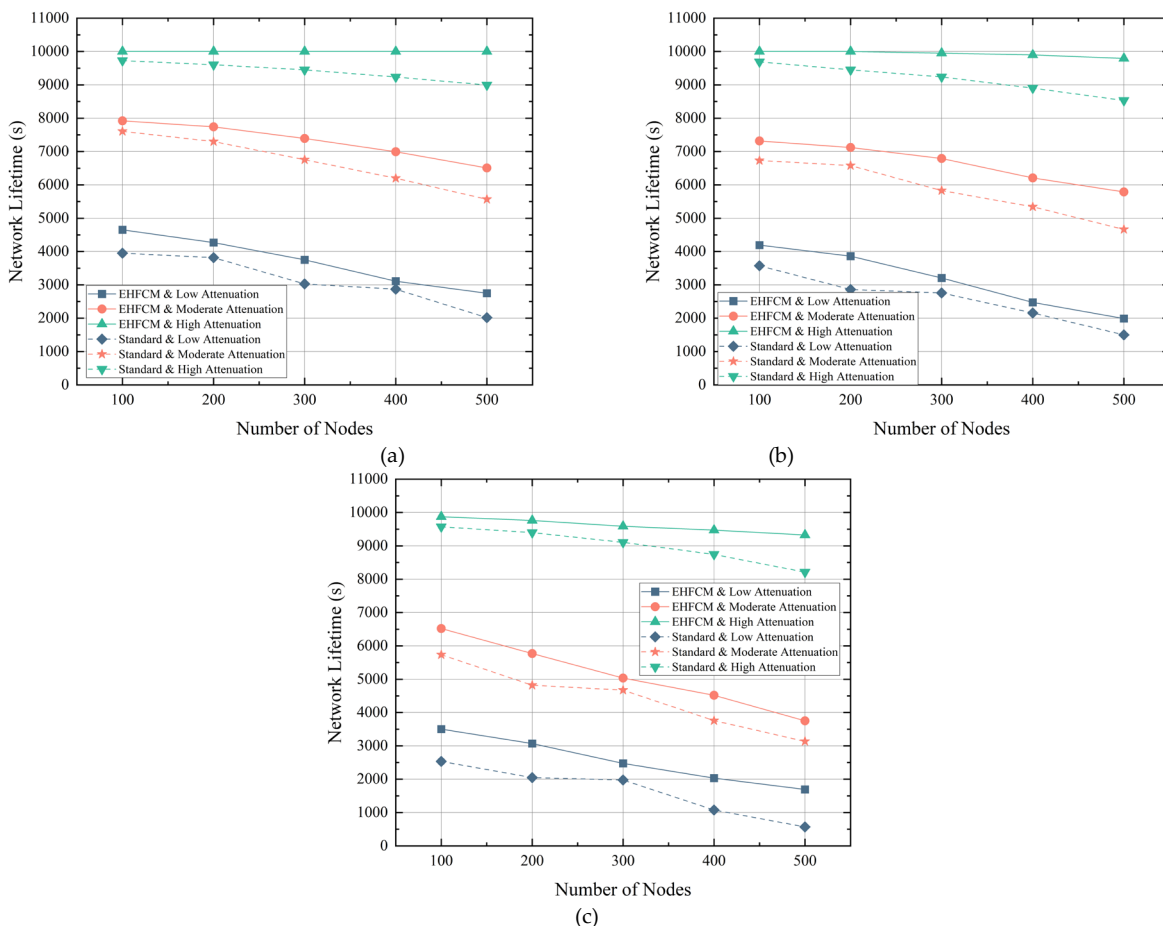


Fig. 12. Network lifetime of EH-FCM based LoRaWAN and standard LoRaWAN for (a) high EH rate, (b) moderate EH rate and (c) low EH rate in different number of nodes.

trajectory that is decidedly more commendable compared to its standard counterpart.

D. Communication Range

This section serves as an extension to the network lifetime analysis presented in Section C, focusing particularly on the deployment cost of sensors, a critical factor in forestry IoT applications. For a fixed sensor count, achieving a broader coverage area while satisfying network lifetime prerequisites contributes to reduced project expenses. The experimental configuration involved 300 sensor nodes, a single gateway, and mandated a minimum 5-meter spacing between sensors. Standard LoRaWAN permits only single-hop communication, whereas the EH-FCM-optimized LoRaWAN supports multi-hop functionality. The network lifetime threshold was established at 2000 seconds, with the transmission range calculated based on the average distance from the gateway to the 50 most remote nodes. Four distinct scenarios were tested, incorporating three specified attenuation types, with a fourth scenario introducing mixed attenuation, indicating variable channel attenuation across different geographical sectors. Data acquisition was based on the mean of 25 independent trials, with findings depicted in Fig. 13 and TABLE III.

The outcomes highlight a discernible expansion in the communication radius within the EH-FCM-enhanced network. Statistical evaluations corroborate a superior stability level within the proposed algorithm. Relative to conditions of low, moderate, and high network channel attenuation, the algorithm facilitated a mean increase in communication distance by 28.17%, 38.33%, and 53.56%, respectively. Under mixed conditions, performance saw a 40.78% boost, culminating in an aggregate enhancement of 40.21%. Such advancements are instrumental for cost-effective LPWAN deployment in forested terrains.

V. CONCLUSION

This study introduces an innovative cross-layer optimization framework, EH-FCM, for LPWANs. The primary focus of this methodology lies in the utilization of FCM to address the conventional challenge of protocol inflexibility across different layers, which often hampers adaptation to the dynamic variables inherent in real-world deployment environments. Additionally, this paper proposes the AGSO algorithm, specifically designed to compute inter-nodal weights within the FCM with heightened efficiency. Experiments show that AGSO has advantages over other intelligent optimization algorithms in terms of convergence and accuracy as well as avoidance of local optimal solutions. Furthermore, comprehensive comparative analysis is conducted between the EH-FCM LoRaWAN and its standard counterpart. The findings highlight the superiority of the EH-FCM approach across various performance metrics, confirming its applicability for tangible forestry implementations. Future research endeavors will focus on the development of an intricate multi-layered FCM, aimed at further enhancing the network efficacy of LPWANs when utilized in conjunction with Unmanned Aerial Vehicles (UAVs).

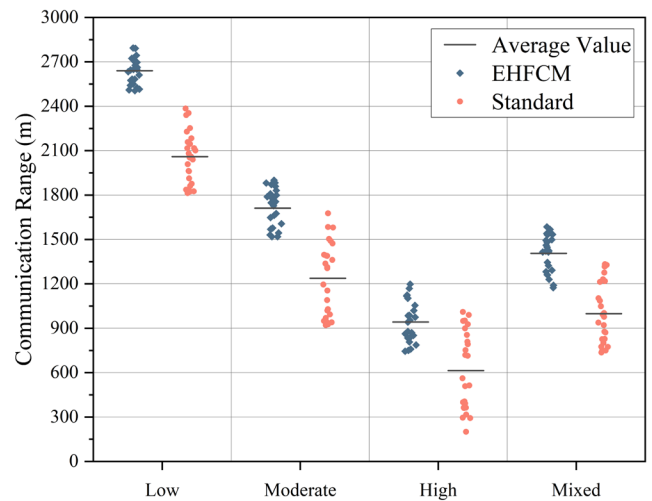


Fig. 13. The communication range in different signal attenuation scenarios.

REFERENCES

- [1] R. Singh, A. Gehlot, S. Vaseem Akram, et al. "Forest 4.0: Digitalization of forest using the internet of things (IoT)," *Journal of King Saud University - Computer and Information Sciences*, vol. 34, no. 8, pp. 5587-5601, Sep. 2022.
- [2] M. Henry et al., "An overview of existing and promising technologies for national forest monitoring," *Annals of Forest Science*, vol. 72, no. 6, pp. 779-788, September 2015.
- [3] N. S. Chilamkurthy, O. J. Pandey, A. Ghosh, L. R. Cengeramaddi and H. -N. Dai, "Low-Power Wide-Area Networks: A Broad Overview of Its Different Aspects," *IEEE Access*, vol. 10, pp. 81926-81959, 2022
- [4] C.-W. Yau et al., "NB-IoT Coverage and Sensor Node Connectivity in Dense Urban Environments: An Empirical Study," *ACM Transactions on Sensor Networks (TOSN)*, vol. 18, no. 3, pp. 1-36, 2022.
- [5] J. Rubio-Aparicio and J. Santa, "An Embedded Crowdsensing Unit for Mobile Urban Pollution Monitoring," *IEEE Communications Magazine*, vol. 61, no. 1, pp. 90-96, January 2023.
- [6] Absar-Ul-Haque Ahmar, Thien Duc Nguyen, Wouter Joosen and Danny Hughes, "EH-CRAM: A Sustainable Energy Harvesting Algorithm for LPWANs," in *Proc. 2019 IEEE Wireless Communications and Networking Conference (WCNC)*, pp. 1-7, March 2021.
- [7] D. K. Sah, A. Hazra, R. Kumar and T. Amgoth, "Harvested Energy Prediction Technique for Solar-Powered Wireless Sensor Networks," *IEEE Sensors Journal*, vol. 23, no. 8, pp. 8932-8940, 15 April, 2023.
- [8] J. Konecny, M. Prauzek and T. Paterova, "Double Q-learning Adaptive Wavelet Compression Method for Data Transmission at Environmental Monitoring Stations," *2022 IEEE Symposium Series on Computational Intelligence (SSCI)*, pp. 567-572, 2022.
- [9] A. Osorio, M. Calle, J. D. Soto and J. E. Candelo-Becerra, "Routing in LoRaWAN: Overview and Challenges," *IEEE Communications Magazine*, vol. 58, no. 6, pp. 72-76, June 2020.
- [10] Carmen Delgado and Jeroen Famaey, "Optimal Energy-Aware Task Scheduling for Batteryless IoT Devices," *IEEE Transactions on Emerging Topics in Computing*, vol.10, no.3, pp.1374-1387, July 2022.
- [11] Mehmet Erkan Yuksel and Huseyin Fidan, "Energy-aware system design for batteryless LPWAN devices in IoT applications," *Ad Hoc Networks*, vol.122, pp.102625, November 2021.
- [12] Davide Magrin, Martina Capuzzo, Andrea Zanella and Michele Zorzi, "A Configurable Mathematical Model for Single-Gateway LoRaWAN Performance Analysis," *IEEE Transactions on Wireless Communications*, vol.21, no.7, pp.5049-5063, July 2022.
- [13] Jerline Sheebha Anni, Arun Kumar Sangaiah, "Wireless Integrated Sensor Network: Boundary Intellect system for elephant detection via cognitive theory and Fuzzy Cognitive Maps," *Future Generation Computer Systems*, vol 83, pp. 522-534, 2018.
- [14] C. Gomez, A. Minaburo, L. Toutain, D. Barthel and J. C. Zuniga, "IPv6 over LPWANs: Connecting Low Power Wide Area Networks to the Internet (of Things)," *IEEE Wireless Communications*, vol. 27, no. 1, pp.

- 206-213, February 2020.
- [15] Mekki K, Bajic E, Chaxel F, et al, "A comparative study of LPWAN technologies for large-scale IoT deployment," *ICT express*, vol. 5, no. 1, pp. 1-7, March 2019.
- [16] A. Ikpehai, B. Adebisi, K. M. Rabie, K. Anoh, R. E. Ande, M. Hammoudeh, H. Gacanin, and U. M. Mbanaso, "Low-power wide area network technologies for Internet-of-Things: A comparative review," *IEEE Internet of Things Journal*, vol. 6, no. 2, pp. 2225-2240, Apr. 2019.
- [17] W. Ayoub, A. E. Samhat, F. Nouvel, M. Mroue, and J.-C. Prévotet, "Internet of mobile things: Overview of LoRaWAN, DASH7, and NB-IoT in LPWANs standards and supported mobility," *IEEE Communications Surveys and Tutorials*, vol. 21, no. 2, pp. 1561-1581, 2nd Quarter, 2019.
- [18] Matasov V, Bellelli Marchesini L, Yaroslavtsev A, et al, "IoT monitoring of urban tree ecosystem services: Possibilities and challenges," *Forests*, vol. 11, no. 7, pp. 775, 2020.
- [19] Callebaut G, Ottoy G, Van der Perre L, "Cross-layer framework and optimization for efficient use of the energy budget of IoT Nodes," *Proc. 2019 IEEE Wireless Communications and Networking Conference (WCNC)*, pp. 1-6, April 2019.
- [20] Mike O. Ojo, Davide Adami, Michele Pagano, et al, "Design, Implementation and Evaluation of a LoRa Packet Generator for Forest Environments," *Proc. 2021 IEEE 26th International Workshop on Computer Aided Modeling and Design of Communication Links and Networks (CAMAD)*, pp. 1-6, October 2021.
- [21] Adomo D, Soares S, Lima J, et al, "Evaluation of LP-WAN technologies for fire forest detection systems," in *Proc. 4th International Conference on Advances in Sensors, Actuators, Metering and Sensing*, pp. 49-53, February 2019.
- [22] O. Elijah, T. A. Rahman, I. Orikumhi, C. Y. Leow, and M. N. Hindia, "An overview of Internet of Things (IoT) and data analytics in agriculture: Benefits and challenges," *IEEE Internet of Things Journal*, vol. 5, no. 5, pp. 3758-3773, October 2018.
- [23] B. Su, Z. Qin and Q. Ni, "Energy Efficient Uplink Transmissions in LoRa Networks," *IEEE Transactions on Communications*, vol. 68, no. 8, pp. 4960-4972, August 2020.
- [24] A. Abouzarkhanifard, H. E. Chimeh, M. A. Janaideh and L. Zhang, "FEMInclusive Transfer Learning for Bistable Piezoelectric MEMS Energy Harvester Design," *IEEE Sensors Journal*, vol. 23, no. 4, pp. 3521-3531, 15 February 2023.
- [25] A. Abouzarkhanifard, H. E. Chimeh, M. Al Janaideh, T. Zou and L. Zhang, "Transfer-Learning-Aided Optimization for a Low-Frequency Wideband MEMS Energy Harvester," *2022 IEEE Sensors*, Dallas, TX, USA, 2022, pp. 1-4.
- [26] Parsi B, Abouzarkhanifard A, Zhang L. "Design and optimization of piezoelectric actuators for microflap-embedded micropumps," *Advances in Mechanical Engineering*, 2023;15(5).
- [27] B. Karg and S. Lucia, "Towards low-energy, low-cost and high-performance IoT-based operation of interconnected systems," in *Proc. 2018 IEEE 4th World Forum on Internet of Things (WF-IoT)*, February 2018, pp. 706-711.
- [28] J. Finnegan, K. Niotaki and S. Brown, "Exploring the Boundaries of Ambient RF Energy Harvesting With LoRaWAN," *IEEE Internet of Things Journal*, vol. 8, no. 7, pp. 5736-5743, 1 April, 2021.
- [29] A. I. Petrariu, A. Lavric, E. Coca and V. Popa, "Hybrid Power Management System for LoRa Communication Using Renewable Energy," *IEEE Internet of Things Journal*, vol. 8, no. 10, pp. 8423-8436, May 2021.
- [30] Carmen Delgado, José María Sanz, Chris Blondia and Jeroen Famaey, "Batteryless LoRaWAN Communications Using Energy Harvesting: Modeling and Characterization," *IEEE Internet of Things Journal*, vol. 8, no. 4, pp. 2694-2711, February 2021.
- [31] Dalibor Purkovic, Marian Hönsch and Tobias Raphael Maria Karl Meyer, "An Energy Efficient Communication Protocol for Low Power, Energy Harvesting Sensor Modules," *IEEE Sensors Journal*, vol. 19, no. 2, pp. 701-714, January 2019.
- [32] Laura Joris, François Dupont, Philippe Laurent, et al, "An Autonomous Sigfox Wireless Sensor Node for Environmental Monitoring," *IEEE Sensors Letters*, vol. 3, no. 7, Article Number 5500604, July 2019.
- [33] Yin Wu and Wenbo Liu, "Routing protocol based on genetic algorithm for energy harvesting-wireless sensor networks," *IET Wireless Sensor Systems*, vol. 3, no. 2, pp. 112-118, June 2013.
- [34] Y. Liu, Y. He, M. Li, J. Wang, K. Liu and X. Li, "Does Wireless Sensor Network Scale? A Measurement Study on GreenOrbs," *IEEE Transactions on Parallel and Distributed Systems*, vol. 24, no. 10, pp. 1983-1993, October 2013.
- [35] Fang R, Wang J, Sun W, "Cross-layer control of wireless sensor network for smart distribution grid," *International Journal of Sensor Networks*, vol. 27, no. 2, pp.71-84, 2018.
- [36] Marini R, Mikhaylov K, Pasolini G, et al, "LoRaWanSim: A flexible simulator for LoRaWAN networks," *Sensors*, vol. 21, no. 3, pp. 695, 2021.
- [37] Petalas Y G, Parsopoulos K E, Vrahatis M N, "Improving fuzzy cognitive maps learning through memetic particle swarm optimization," *Soft Computing*, vol. 13, no. 1, pp. 77-94, 2009.
- [38] Ye N, Gao M, Zhang R, et al, "Learning sparse fuzzy cognitive maps by ant colony optimization," *2013 10th International Conference on Fuzzy Systems and Knowledge Discovery (FSKD)*. IEEE, pp. 68-76, 2013.
- [39] Chen Y, Mazlack L J, Minai A A, et al, "Inferring causal networks using fuzzy cognitive maps and evolutionary algorithms with application to gene regulatory network reconstruction," *Applied Soft Computing*, vol. 37, pp. 667-679, 2015.
- [40] Malayjerdi E, Yaghoobi M, Kardan M, "Mobile robot navigation based on fuzzy cognitive map optimized with grey wolf optimization algorithm used in augmented reality," *2017 5th RSI International Conference on Robotics and Mechatronics (ICRoM)*. IEEE, pp. 211-218, 2017.